Desalination and Water Treatment
www.deswater.com

doi:10.5004/dwt.2018.22940

131 (2018) 212–219
November

Novel synthesis and enhanced catalytic performance of stable nano-scale Fe^0, Ag^0 and ZnO nanoparticles: photo-degradation under mercury lamp

Sadia Ata[a], Muhammad Zafar Ullah[a,b], Muhammad Imran Din[a,*], Rashad Mehmood[b], Wasif Farooq[c], Syed Ahmed Trimzi[d], Ismat Bibi[e]

[a]*Institute of Chemistry, University of the Punjab, Lahore-54590, Pakistan, email: sad_ziam@yahoo.com(S. Ata), zafarullah298@gmail.com(M. Zafar Ullah), Cell: +92-3007818870, Fax +92-42-99231269, email: imrandin2007@gmail.com (M.I. Din)*
[b]*Department of Chemistry, University of Education, Vehari Campus, Vehari-61100, Pakistan, email: rashadhej@gmail.com (R. Mehmood)*
[c]*Department of Chemistry, National University of Science and Technology (NUST), Islamabad, Pakistan, email: wasif.farooq@scme.nust.edu.pk (W. Farroq)*
[d]*Department of Chemistry, Quaid-e-Azam University, Islamabad, Pakistan, email: satirmizi_qau@yahoo.com (S.A. Tirmzi)*
[e]*Department of Chemistry, The Islamia University of Bahawalpur, Bahawalpur-63100, Pakistan, email: ismat16_08_1982@yahoo.com (I. Bibi)*

Received 19 November 2017; Accepted 12 August 2018

ABSTRACT

This study was planned to synthesize the Fe^0, Ag^0 and ZnO nanoparticles (NPs) and measure their catalytic potential to degrade the industrial pollutants into non-pollutant materials. Iron and silver NPs have been obtained through leaf extract of *Azadirachta indica* and ZnO NP has been synthesized over leaf extract of *Corriandrum sativum* as single step, simple, cheap and eco-friendly green synthesis. The synthesized NPs were confirmed by UV-visible spectroscopy and further characterized by scanning electron microscopy (SEM), energy dispersive X-Ray spectroscopy (EDS), fourier transform infrared spectroscopy (FTIR) and X-ray diffraction (XRD). The photocatalytical potential of the synthesized NPs was measured as photodegration of methyl orange (MO) azodye as model organic compound under high pressure mecury lamp of 125 W and 500 W. The photodegradation was 24%, 30% and 51% after 4.5 h at 125 W and 56%, 60% and 83% after 4 h at 500 W for silver, iron and zinc oxide NPs, respectively. Catalytic potential of ZnO was better with 0.47 and 0.087 absorbances as compared to silver and iron NPs under both 125 W and 500 W, respectively. The potential of ZnO NPs was much better at 500 W than 125 W. The optimum degradation of methyl orange with ZnO NPs was observed at 0.6 g/L, and acidic pH (=3) further enhance and hasty the degradation. Consequently, 98.5% MO was degraded at 3 pH and 500 W. The plausible mechanism of photodegradationwas also discussed.

Keywords: Synthesis of Fe, Ag, and ZnO NPs; Plant mediated eco-friendly synthesis; Photocatalytic potential; Effect of power of lamp and pH

---

1. Introduction

Azo compounds are extensively used as organic dyes in textile industries [1]. After dying, around 15 % of azo dyes are lost or remained in the effluents. These dyes are toxic for our ecosystem, particularly for microorganisms. These organic dyes required a long time for natural degradation and biological degradation is unaffected for many azo dyes. So, these dyes should have to be eliminated chemically from industrial effluents before discharge in environment. Numerous methods have been reported for the treatment of waste water such as biodegradation [2], photodegradation [3–5] and absorptional-photodegradation [6]. Nano-sized particles are attractive as catalysts due to their high reac-

---

*Corresponding author.

tivity and attributed to enhanced surface area to chemically degrade these organic pollutants or dyes [7,8]. Reactive surfaces are applied as semiconductor-based membranes activated by UV or sunlight to participate in redox processes for the degradation of organic compounds in wastewater. Nanoparticles of metal oxides [9] and semiconductors are of great attention due to novel properties compared to their bulk materials [10,11]. Semiconductor NP shaveability to degrade dyes from industrial effluents through photo-catalysis [12,13], as these nanoparticles possess unique mechanical, optical and electrical properties. Among various semiconductor nanoparticles, ZnONPs are frequently used because of their applications in chemical sensor, electrostatic, dissipative coating, luminescence, transparent UV-protection films, photo-catalysis and solar energy conversion. Photo-catalysis involves the complete conversion of toxic dyes into CO_2, H_2O and other inorganic compounds that are nontoxic, and other advantage of photocatalysis is that it does not produce secondary pollution. Semiconductors have broad band gap [14] and ultraviolet light ($\lambda <$ 350 nm) is used for the activation of band gap of semiconductors. There is a limitation for degradation by sunlight, because only 3–4% of solar light fall in UV region [15,16]. Different semiconductors can be coupled to get disparate width of band gaps to enhance photocatalytic activity of semiconductors [16–20]. There is a tendency of agglomeration of nanomaterials in aqueous solution during usage and preparation by inter particle synergistic effect (e.g. vander waals interaction). There is also a limitation in recovery of nano-sized materials used in photo degradation.

In recent years, much research is going on metallic nanoparticle and its properties like catalyst, sensing to optics, antibacterial activity, data storage capacity, etc. [21,22]. Different physical and chemical methods including green synthesis are used to prepare various NPs [23,24] such as silver and gold NPs were prepared by using extracts of vaious plant species [25–28].

Literature shows that ZnO NPs has good potential to degrade the various azo dyes [29,30]. So, ZnO was selected to check its potential against current selected azo dye and compare its potential with the Fe and Ag nanoparticles. Hence, here we report the synthesis of iron, silver and zinc oxide nanomaterials under mild plant mediated conditions and they were characterized by UV-visible, SEM, XRD and FTIR. Photo-catalytic potential of the synthesized Fe, Ag and ZnO NPs was measured through degradation of methyl orange, which is a harmful azodye. As a result, ZnO NPs are better photocatalyis than Fe and Ag NPs, showed even better degradation at high power of lamp and acidic pH and it can be used to eliminate the azo dye from industrial waste effluents.

2. Experimental

2.1. Materials and methods

Ferric chloride, silver nitrate, zinc acetate, and liquid ammonia were purchased from Merck and sodium hydroxide, methyl orange and ethanol from Sigma. UV-Vis spectra were measured through dispersion on Shimadzu UV-Vis-240 spectrophotometer whereas FTIR spectra were meaured as KBr pelletson JASCO, FTIR-460 plus, SEM images were determined on JEOL, JSM-6701F and XRD were analyzed on (X'Pert Pro, Philips X-ray diffractometer) and photocatalytic degradation were determined on UV-Vis spectrophotometer (Perkin Elmer Lambda 11) with high pressure mercury lamp at 125 W and 500 W.

2.2. Synthesis of Iron (Fe^0) and Silver (Ag^0) Nanoparticles

Fresh leaves of *Azadirachta indica* (local name: Neem) were accumulated locally, cleaned with distilled water and chopped into small pieces. The chopped leaves were boiled in distilled water, filtered it and collected the filtrate. $FeCl_3$ Solution (0.1 M) and $AgNO_3$ solution (0.01 M) were separately mixed with leaf filtrate in appropriate ratio (1:4). In the case of $FeCl_3$: color immediately changed after mixing and the mixture was further heated for half an hour at 70°C and precipitates appeared. Then these precipitates were separated through centrifugation as iron nanoparticles and these nanoparticles were dried in an oven at 70°C. In the case of $AgNO_3$: pH 8 was maintained by adding dilute ammonium hydroxide and flask was rotated at 80 rpm at rotatory shaker for four hours. Ag NPs were obtained by centrifuge and dried in oven at 70°C.

2.3. Synthesis of Zinc oxide NPs (ZnO)

Fresh leaves of *Corriandrum sativum* (local name: Dhanya) were collected locally, cleaned with distilled water and chopped into small pieces. The chopped leaves were boiled in distilled water, filtered it and collected the filtrate. 100 mL of zinc acetate (0.02 M) was mixed in 50 mL distilled water by vigorous and continuous stirring and then it mixed with leaf filtrate in appropriate ratio (1:4). pH was maintained by adding sodium hydroxide (2 M) and the mixture magnetically stirred for 2 h. After 2 h precipitates appeared and settle down the precipitates for 2 h. Then precipitates were filtered, washed and dried in oven for 20 min at 200°C. Pale white nanoparticles were obtained after calcination.

3. Results and discussion

Fe and Ag NPs were prepared by *Azadirachta indica* leaf extract mediated and ZnO NPs were prepared by *Corriandrum sativum* leaf extract mediated. The prepared NPs were characterized by UV-Vis, SEM, XRD and FTIR, and check their photo-degradation potential through high pressure mercury lamp (125 W and 500 W).

3.1. UV-Vvisible spectrum of nanoparticles

UV-visible spectroscopy was used to confirm the existance of Fe, Ag and ZnO nanoparticles. The UV-VIS spectrum of iron NPs showed the absorption maxima at 352 nm (Fig. 1a) due to the SPR (surface plasmon resonance), which was similar to the reported value for iron NPs [31] and confirming the existence of iron NPs. The UV-Vis spectrum of silver nanoparticles showed maximum absorption at 455 nm (Fig. 1b), which was compareable to the reported data for Ag NPs [32] and this indicating the existence of silver NPs. The UV-Vis spectrum of ZnO nanoparticles exhibited the strong absorption peak at 330 nm (Fig. 1c), which is similar to the reported value for ZnO NPs [33] and confirming the presence of ZnONPs. Blue shifts were observed of all these nano sizes particles when compared with their non-nano sized particles.

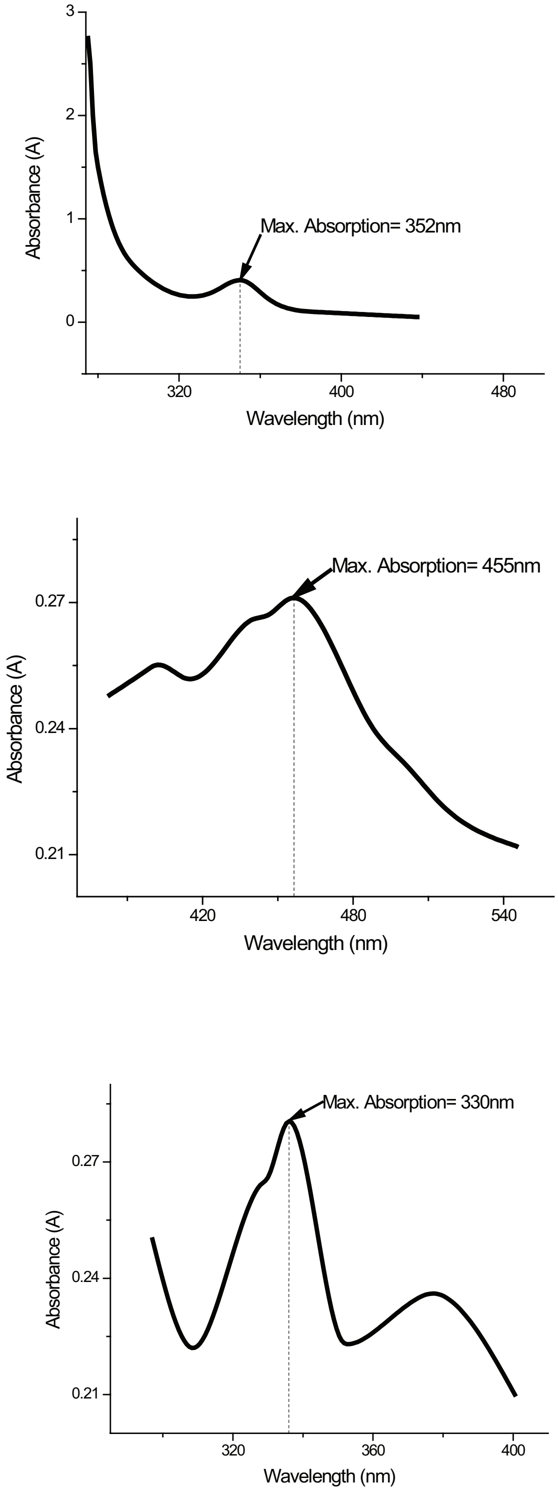

Fig. 1. (a). UV-VIS spectrum of FeNPs (b). UV-VIS spectrum of Ag NPs, (c). UV-VIS spectrum of ZnONPs.

3.2. Scanning electron microscopy (SEM)

Morphology of the newly synthesized iron, silver and zinc oxide nanoparticles was confirmed by SEM., 40000 and 60000 magnifications, and 0.5 µm and 0.2 µm resultion were used to confirm the sizes of the nanoparticles.

SEM image of iron NPs (Fig. 2a) shows a size distribution of 25 nm to 40 nm and SEM images of iron nanoparticles show homogeneous distribution of the particles. SEM image of silver NPs (Fig. 2b) shows the size of the particles which is within the range of 29 nm to 37 nm and have homogeneous distribution. SEM represents and confirms the nano sized material of ZnO. A structural feature of ZnO-NPs shows that they are crystalline, granular and they possesses diameter 30 nm to 64 nm as appeared from SEM images (Fig. 2c). All SEM results confirmed that prepared particles are of nano sized have diameters as iron NPs have 25–40 nm, silver NPs have 29–37 and ZnONPs have 30–64 nm.

3.3. EDS (Energy dispersive X-ray spectroscopy)

In case of iron NPs, Fe-Lα, Fe-Kα, Fe-Kb confirms presence of iron nanoparticles. $FeCl_3$ was employed in preparation. It releases chlorine which appears as peak in EDS. Presence of calcium, magnesium and silicon are

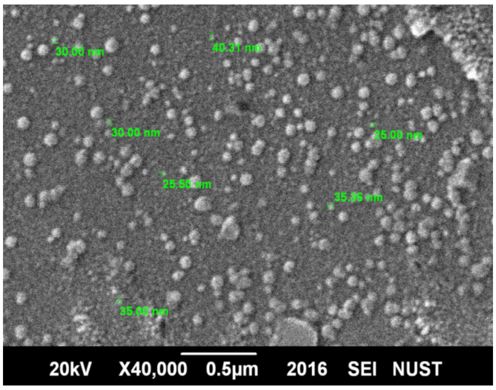

Fig. 2a. SEM of iron nanoparticles at 40,000× magnifications at 0.5 µm resolution.

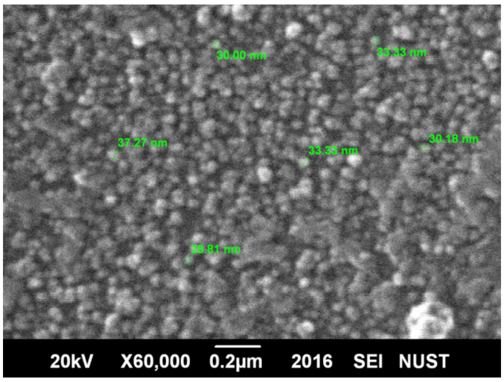

Fig. 2b. SEM images of silver nanoparticles at 60,000× magnifications at 0.2 µm resolution.

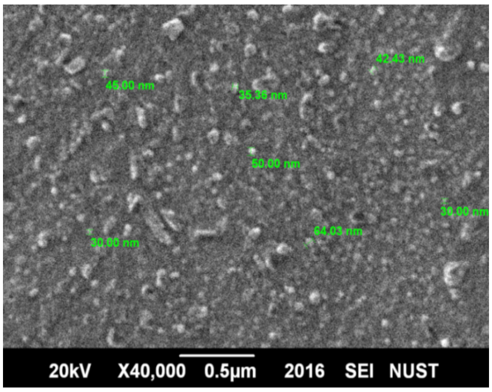

Fig. 2c. SEM of ZnO nanoparticles at 40,000× magnifications at 0.5 μm resolution.

due to green synthesis of nanoparticles. Due to oxidized form of iron, Okα appeared for oxygen in EDS spectrum (Fig. 3a).

AgLα, AgLβ transition occurs in case of silver nanoparticles. Okα peak justifies the formation of oxidized form of silver nanoparticles. EDS is important for elemental analysis. Presence of calcium and magnesium and silicon are due to green synthesis of nanoparticles. These peaks appeared as Kα in EDS spectrum. Magnified image (X75) at 20 kV potential is shown in Fig. 3. Due to improper grinding, nanoparticles appears in attached form (Fig. 3b).

Okα of oxygen appeared with ZnKα, ZnKβ and ZnLα, which indicates presence of ZnO nanoparticles. Gold is used for sputtering and appeared as peak at 2.2 KeV. Nanoparticles possess porous structures and attached with each other in EDS images (Fig. 3c).

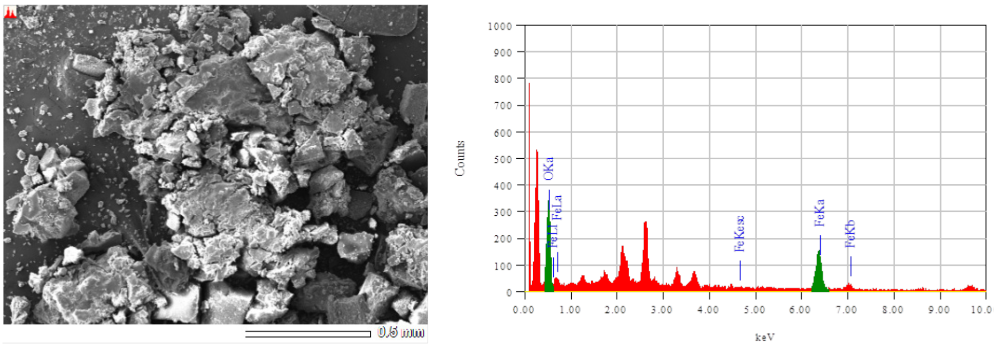

Fig. 3a. EDS image at 0.5 mm resolution and spectrum of iron nanoparticles.

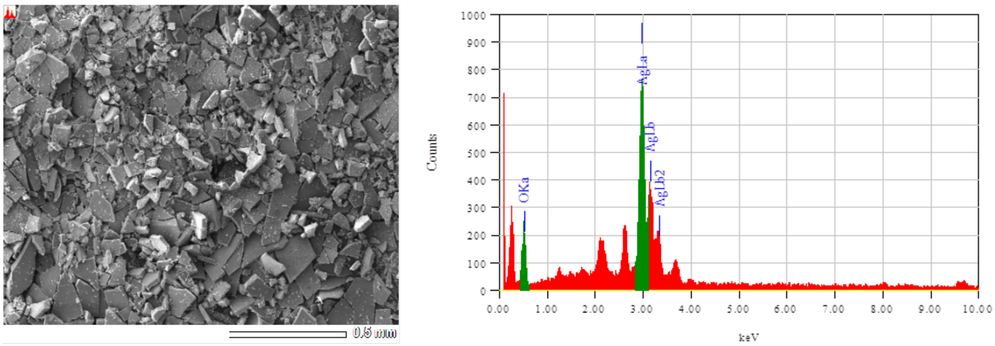

Fig. 3b. EDS image at 0.5 mm resolution and spectrum of silver NPs.

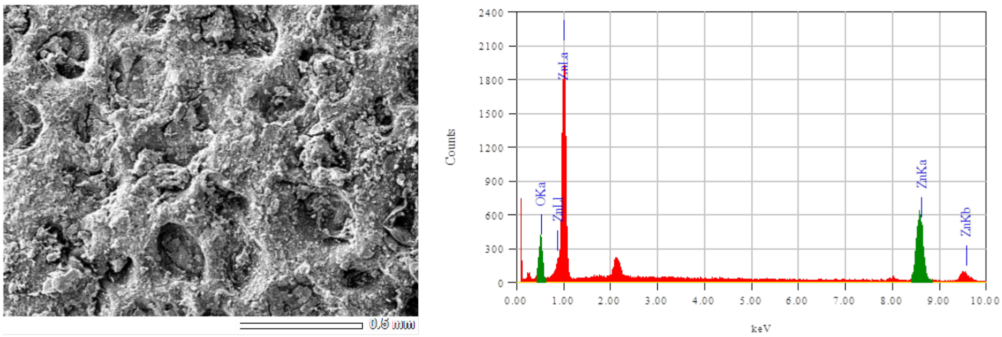

Fig. 3c. EDS image at 0.5 mm resolution and spectrum of ZnO-NPs.

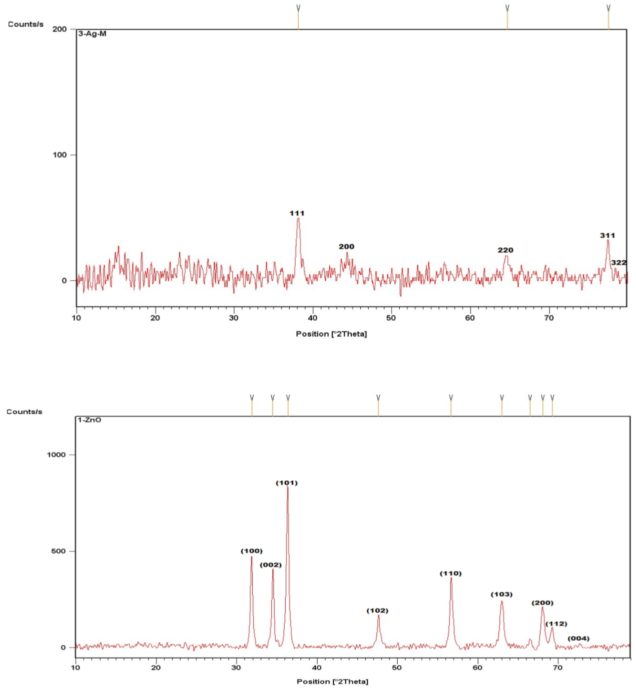

Fig. 4. XRD of Ag NPs (a), ZnONPs (b).

3.4. XRD (X-Ray diffraction analysis)

XRD diffraction pattern for silver nanoparticles is shown in Fig. 4a. Face centered cubic structure appeared from all diffraction of silver nanoparticles. Mean measurement of crystallite was calculated from Debye-scherrer equation [Eq. (1)]. 6.5 nm was mean size of particles.

$$D = \frac{K \cdot \lambda}{\beta cos\theta} \tag{1}$$

Here K is constant (0.89), λ is the X-ray wavelength (1.54 Å), *D* is grain size in nanometer, θ is the half of diffraction angle, β is the full width at half maxima (FWHM).

Sharp and intense peaks appeared for ZnONPs are shown in Fig.4b. Crystalline nature of synthesized particles was verified by X-ray diffraction analysis. Mean size of crystals of ZnONPs can be calculated from Debye-Scherrer equation. Mean particle size is 19 nm calculated from equation and intense peak appeared at 101 plane.

3.5. Fourier transform infrared (FTIR) characterization

FTIR spectrum of iron-NPs is shown in Fig. 5a. The peaks observed at 1053 cm^{-1}, 1627 cm^{-1} and 3433 cm^{-1} are due N-H stretching, O-H stretching, C-H stretching and bending vibrations of NH_2^+group in Neem leaf extract. Presence of iron-NPs is appeared at 425 cm^{-1}. This peak is due Fe-O stretching which suggests that iron is in oxidized form. FTIR of silver nanoparticles is shown in Fig. 5c. Characteristic peak of Ag-O stretching appeared at 433 cm^{-1} and 555 cm^{-1}. Peaks at 1073 cm^{-1} and 1656 cm^{-1} represents NH_2^+group in Neem leaf extract. A peak at 2925 cm^{-1} and 3300–3500 cm^{-1} represents the presence aldehyde and hydroxyl groups that are phytochemicals and enhances the stability of nanoparticles in aqueous medium.

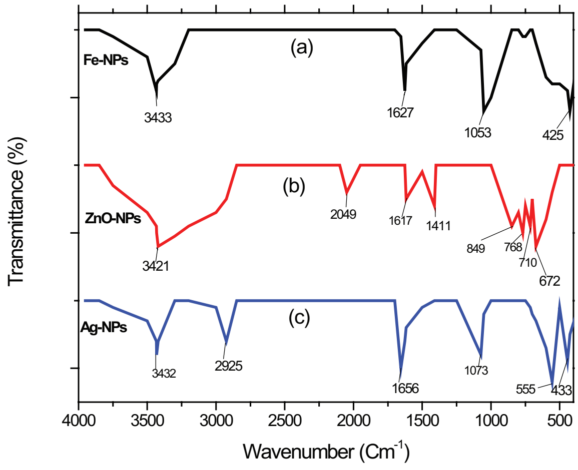

Fig. 5. FTIR of iron, silver and zinc oxide nanoparticles.

Hydroxyl peak stretching vibration was observed at 3300–3500 cm^{-1}. For conversion of $Zn(OH)_2$ into ZnO-NPs, muffle furnace used and calcination was done at 200°C. But minute amount remained in hydroxide form. Characteristic peak of Zn-O stretching vibration was observed at 672 cm^{-1} (Fig. 5b). The pattern of absorption at 710 cm^{-1} and 849 cm^{-1} represents aromatic out of plane C-H stretching. Stretching vibration of C-N amine appeared at 1053 cm^{-1}. Peaks at 1411 cm^{-1} to 1617 cm^{-1} represents the presence of aromatic ring. A peak at 3300–3500 cm^{-1} represents the presence of amines and hydroxyl groups that are phytochemicals and enhances the stability of nanoparticles in aqueous medium.

3.6. Kinetics of photo-degradation of methyl orange (MO) by different photo-catalysts

Photo-degradation potential of the prepared NPs (Fe, Ag & ZnO) were measured under high pressure mercury lamp using two different powers 125 W and 500 W. Photo-degradation potentials of NPs (0.5 g/L, each) were measured with methyl orange solution (15 ppm or 15 mg/L) and the time was adjusted as 4.5 h for 125 W and 4 h for 500 W. Under 125 W mercury lamp, the photodegradation percentages of methyl orange with silver, iron and zinc oxide NPs were 24%, 30% and 51%, respectively, after 4.5 h. The decolorization of methyl orange with each NPs is shown in Fig. 6a, which indicates that ZnO NPs has better photocatalytic potential as compared to Fe and Ag NPs. Under 125 W experimental conditions UV-Visible spectra were also measured (Fig. 6b), and spectrum showed the absorbance of methyl orange original and after degradation with each NPs. The maximum decrease in absorption was observed with the net value 0.47 for ZnONPs at λ_{max} 455 nm. This decrease in absorption of ZnO NPs can be explained on the basis of formation of simple molecule as a result of degradation of MO. So, it is evidence that ZnO NPs betterly degrade the methyl orange, hence has better photocatalytic potential as compared to Fe and Ag NPs.

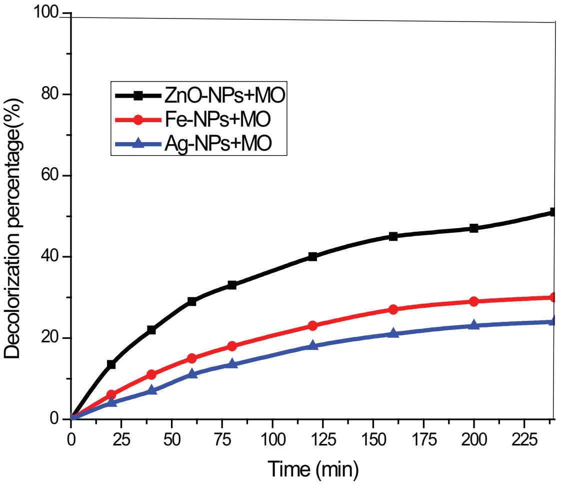

Fig. 6a. Decolonization percentage of MO (15 ppm) under 125 W high pressure mercury lamp..

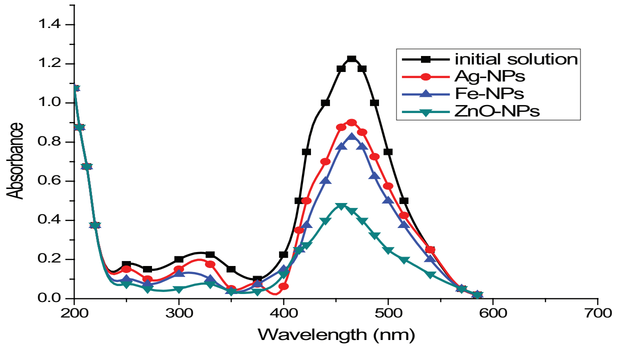

Fig. 6b. UV-visible spectra of methyl orange for different nanomaterials (15 mg/L MO) after 4.5 h photodegradation under 125 W high pressure mercury lamp.

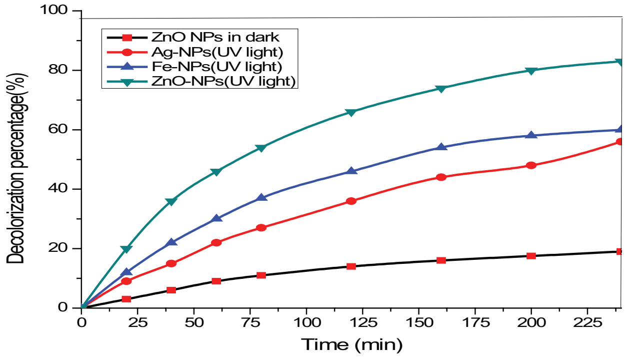

Fig. 6c.Photodegradation of MO (15 ppm) under 500 W high pressure mercury lamp.

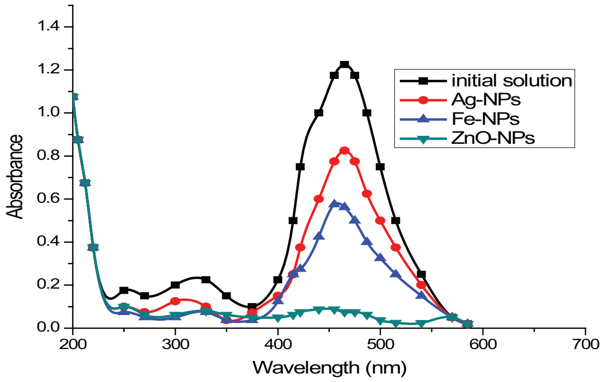

Fig. 6d. UV-visible spectra of methyl orange for different nanomaterials (15 mg/L MO) after 4.5 h photodegradation under 500 W mercury lamp.

Under 500 W of mercury lamp, the photodegradation percentages of methyl orange with silver, iron and zinc oxide NPs were 56%, 60%, and 83%, respectively (Fig. 6c), it indicates the better photocatalytic potential of ZnO NPs as compared to Fe and Ag NPs. Their UV-Visible spectra were also measured which is shown in Fig. 6d. UV-Vis spectrum showed the absorbance of methyl orange original and after degradation with each NPs and maximum decrease in absorption was observed at λ_{max} 455 nm for ZnONPs. The absorption was decreased from 0.47 to 0.087 when power of mercury was increased from 125 W to 500 W. The further decrease in aborption of ZnO NPs at 500 W as compared to 125 W explains that ZnONPs can much betterly degrade the MO at high power (500 W) is used.

As ZnO NPs showed the better photodegradation at both 125 W and 500 W as compared to Fe and Ag NPs, so photocatalytical potential of ZnO NPs was also checked in dark for 4 h and it showed 19% decolorization of MO (Fig. 6c).

3.6. Mechanism for kinetics of photodegradation of MO by different photocatalysts

Expected mechanism for degradation is given below:

$$\text{NPs} + h\upsilon \longrightarrow \text{NPs}^*$$

$$\text{NPs}^* + H_2O \longrightarrow \text{NPs} + H^+ + {}^{\bullet}OH$$

$$^{\bullet}OH + \text{Dye molecule} \longrightarrow CO_2 + H_2O + \text{simple inorganic molecules}$$

3.7. Effect of catalyst amount

ZnO-NPs were used further to investigate the effect of dosage of photo-catalyst due to their better efficiency. Different amounts of photo-catalyst 0.2, 0.4, 0.6, 0.8 and 1g per liter of MO (15 ppm) was prepared. Decolorization percentage was increased with the increase in catalyst amount from 0.2 to 0.6 g/L. However further increase in photo-catalyst amount results in decrease of decolorization percentage (Fig. 7). By increasing the amount of photo-catalyst increases the number of active sites for degradation. Hence, greater number of molecules absorbs UV light and degradation percentage increases. But in excess amount of photo-catalyst agglomeration and blocking of light occurs and light from UV-lamp cannot be penetrated properly into the system. As a result degradation ability of

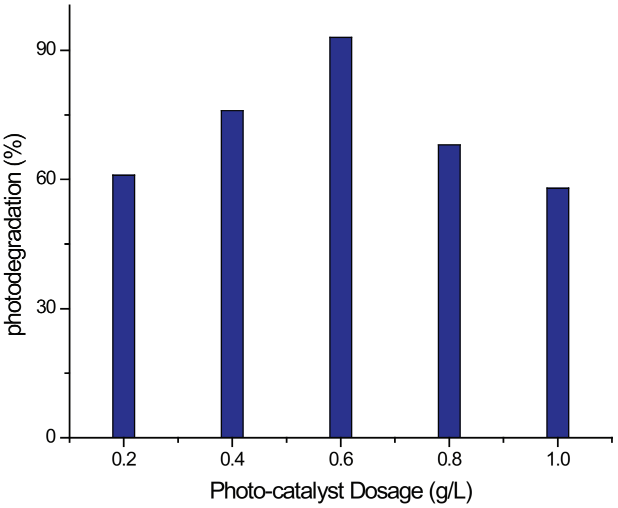

Fig. 7. Effect of ZnO NPs catalyst dosage on photodegradation.

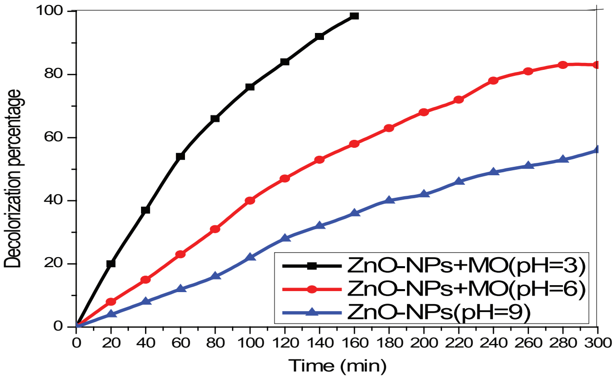

Fig. 8. Effect of pH on photodegradation.

photo-catalyst is decreased. Hence optimum dosage was 0.6g/L was observed for ZnONPs that were much lower as compared to reported TiO_2 nanoparticles as photo-catalyst (2.5g/L) [34].

3.8. Effect of pH

Effect of pH on photodegradation was also measured and it is examined at pH 3, 6, and 9 because pH is one of the important parameter for decolorization of dyes.

Decolorization percentage of methyl orange was attained 98.5, 83 and 56% at pH 3, 6 and 9, respectively, whereas, the previously reported decolorization of MO dye with pure ZnO was up to 85% at pH 5.5 and 0.4 g/L catalyst dose [35]. Furthermore it is point to be noted that at pH 3, NPs took about 160 min to achieve 98.5% degradation (Fig. 8). Point of zero charge pHpzc is important to explain to effect of pH. Due to surface-charge properties of catalyst, the surface of catalyst becomes positively charged at lower pH and as a result the photo-catalytic activity increases. At pH values greater then pHpzc results in decrease of photo-catalytic activity. So acidic pH was suitable for photo-catalytic decolorization of MO dye.

3.9.. Recycling ability of ZnO photocatalyst

Recycling of ZnO catalyst was processed with slight modification method reported in the literature [35]. The sample of photocatalyst was kept first in the dark for 20 min to saturate the absorption of methyl orange dye and then exposed to visible irradiation light. After 100 min, the sample was separated from the test solution by filtering. Same procedure was repeated for second and third time.

4. Conclusion

Fe, Ag and ZnO NPs were synthesized by plant extracts through simple, cheap and eco-friendly green synthesis. Their existence was checked by λ_{max} and morphology by SEM. Their photocatalytic potentials were measured by degrading methyl orange dye under high pressure mercury lamp of 125 and 500 W. The methyl orange photodegradation percentages were 24%, 30% and 51% after 4.5 h at 125 W and 56%, 60% and 83% after 4 h at 500 W for silver, iron and zinc oxide NPs, respectively. ZnONPs showed good catalytic potential at 125 W, whereas excellent potential with 98.5% MO degradation at 500 W as compared to silver and iron NPs. The optimum photocatalyst dosage was 0.6 g/L and optimun pH was 3 to quick (160 min) and maximum MO dye degradation.

References

[1] H. Park, W. Choi, Visible light and Fe(III)-mediated degradation of acid orange 7 in the absence of H_2O_2, J. Photochem. Photobiol. A: Chem., 159 (2003) 241–247.

[2] S. Palamthodi, D. Patil, Y. Patil, Microbial degradation of textile industrial effluents, African. J. Biotech., 10 (2011) 12657–12661.

[3] A. Kumar, A. Kumar, G. Sharma, M. Naushad, F.J. Stadler, A.A. Ghfar, P. Dhiman, R. Saini, Sustainable nano-hybrids of magnetic biochar supported $g\text{-}C_3N_4/FeVO_4$ for solar powered, degradation of noxious pollutants- Synergism of adsorption, photocatalysis & photo-ozonation, J. Clean. Prod., 165 (2017) 431–451.

[4] A. Kumar, G. Sharma, M. Naushad, R. Cataluna, F.J. Stadler, A. Kumar, A.A. Ghfar, M.R. Khan, Solar-driven photodegradation of 17-β-estradiol and Ciprofloxacin from waste water and CO_2 conversion using sustainable Coal-char/polymeric-g-C_3N_4/RGO metal free nano-hybrids, New J. Chem., 41 (2017) 10208–10224.

[5] G. Sharma, S. Bhogal, M. Naushad, Inamuddin, A. Kumar, F.J. Stadler, Microwave assisted fabrication of La/Cu/Zr/carbon dots trimetallicnanocomposites with their adsorptional vs photocatalytic efficiency for remediation of persistent organic pollutants, J. Photochem. Photobio. A: Chem., 347 (2017) 235–243.

[6] D. Pathania, D. Gupta, A.H. Al-Muhtaseb, G. Sharma, A. Kumar, M. Naushad, T. Ahamad, S.M. Alshehri, Photocatalytic degradation of highly toxic dyes using chitosan-g-poly(acrylamide)/ZnS in presence of solar irradiation, J. Photochem. Photobio. A: Chem., 329 (2016) 61–68.

[7] B.J. Hinds, N. Chopra, T. Rantell, R. Andrews, V. Gavalas, L.G. Bachas, Aligned multiwalled carbon nanotube membranes, Science, 303 (2004) 62–65.

[8] H.S. Lee, S.J. Im, J.H. Kim, H.J. Kim, J.P. Kim, B.R. Min, Polyamide thin-film nanofiltration membranes containing TiO_2 nanoparticles, Desalination, 219 (2008) 48–56.

[9] A. Srivastava, O.N. Srivastava, S. Talapatra, R. Vajtai, P.M. Ajayan, Carbon nanotube filters, Nat. Mater., 3 (2004) 610–614.

[10] H.D. Raval, J.M. Gohil, Nanotechnology in water treatment: an emerging trend, Int., J. Nuclear Desal., 4 (2010) 184–188.

[11] R.S. Samuel, K. Sridharan, Water remediation by nanofiltration and catalytic degradation, in emerging trends of nanotechnology in environment and sustainability: a review-based approach, edited by K. Sridharan, Published by Springer Nature, Gewerbestrasse, 2018, 99–106.
[12] U.G. Akpan, B.H. Hameed, Parameters affecting the photocatalytic degradation of dyes using TiO_2-based photocatalysts: a review, J. Hazard. Mater., 170 (2009) 520–529.
[13] M. Makita, A. Harata, Photocatalytic decolorization of rhodamine B dye as a model of dissolved organic compounds: influence of dissolved inorganic chloride salts in seawater of the Sea of Japan, Chem. Eng. Process., 47 (2008) 859–863.
[14] S. Kaur, V. Singh, Visible light inducing sonophotocatalytic degradation of reactive red dye 198 using dye sensitized TiO_2, Ultrason. Sonochem., 14 (2007) 531–537.
[15] W. Liu, S. Chen, W. Zhao, S. Zhang, Study on the photocatalytic degradation of trichlorfon in suspension of titanium dioxide, Desalination, 249 (2009) 1288–1293.
[16] M.A. Behnajady, N. Modirshahla, R. Hamzavi, Kinetic study on photocatalytic degradation of C.I. Acid Yellow 23 by ZnO photocatalyst, J. Hazard. Mater., 133 (2006) 226–232.
[17] S.K. Kansal, M. Singh, D. Sud, Studies on TiO_2/ZnO photocatalysed degradation of lignin, J. Hazard. Mater., 153 (2008) 412–417.
[18] D.L. Liao, C.A. Badour, B.Q. Liao, Preparation of nanozied TiO_2/ZnO composite catalyst and its photocatalytic activity for degradation of methyl orange, J. Photochem. Photobiol. A, 194 (2008) 11–19.
[19] X.D. Yu, Q.Y. Wu, S.C. Jiang, Y.H. Guo, Nanoscale ZnO/TiO_2 composites: preparation, characterization and visible-light photocatalytic activity, Mater. Charact., 57 (2006) 333–341.
[20] A.A. Aal, M.A. Barakat, R.M. Mohamed, Electrophoreted Zn–TiO_2–ZnO nanocomposite coating films for photocatalytic degradation of 2-chlorophenol, Appl. Surf. Sci., 254 (2008) 4577–4583.
[21] M.M. Kholoud, A.E. Nour, A. Eftaiha, Abdulrhman, Al-Warthan Reda, A.A. Ammar, Synthesis and applications of silver nanoparticles, Arab. J. Chem., 3 (2010) 135–140.
[22] K.V. Sharma, A.R. Yngard, Y. Lin, Silver nanoparticle: Green synthesis and their antimicrobial activities, Adv. Colloid Inter. Sci., 145 (2009) 83–96.
[23] M. Darroudi, M.B. Ahmad, A.K. Zak, R. Zamiri, Hakimi, Fabrication and characterization of gelatin stabilized silver nanoparticles under UV-light, Int. J. Mol. Sci., 12 (2011) 6346 6356.
[24] D.S. Kilin, O.V. Prezhdo, Y.N. Xia, Shape-controlled synthesis of silver nanoparticles: Ab *in vitro* study of preferential surface coordination with citric acid, Chem. Phys. Lett., 458 (2008) 113–116.
[25] S.S. Shankar, A. Ahmad, M. Sastry, Geranium leaf assisted biosynthesis of silver nanoparticles, Biotechnol. Prog., 19 (2003) 1627–1631.
[26] N. Ahmad, S. Sharma, V.N. Singh, S.F. Shamsi, A. Fatma, B.R. Mehta, Biosynthesis of silver nanoparticles from desmodium-triflorum: a novel approach towards weed utilization, Biotechnol. Res. Int., 2011 (2011) pages 10.
[27] H. Bar, D.K. Bhui, G.P. Sahoo, P. Sarkar, S.P. De, A. Misra, Green synthesis of silver nanoparticles using latex of *jatrophacurcas,* Colloids Surf. a: Physicochem. Engineering Aspects, 339 (2009) 134–139.
[28] J.A.J. Paul, B.K. Selvi, N. Karmegam, Biosynthesis of silver nanoparticles from *Premnaserratifolia* L. leaf and its anticancer activity in CCl_4-induced hepato-cancerous Swiss albino mice, Appl. Nanosci., 5 (2015) 937–944.
[29] P. Gonçalves, R. Bertholdo, J.A. Dias, S.C. Maestrelli, T.R. Giraldi, Evaluation of the photocatalytic potential of TiO_2 and ZnO obtained by different wet chemical methods, Mater. Res., 20 (2017) 181–189.
[30] S.K. Kansal, N. Kaur, S. Singh, Photocatalytic degradation of two commercial reactive dyes in aqueous phase using nanophotocatalysts, Nanoscale Res.Lett., 4 (2009) 709–716.
[31] K. Klačanová, P. Fodran, P. Šimon, P. Rapta, R. Boča, V. Jorík, M. Miglierini, E. Kolek, L'. Čaplovič, Formation of Fe(0)-nanoparticles via reduction of Fe(II) compounds by amino acids and their subsequent oxidation to iron oxides, J. Chem., 2013, 2013, Article ID 961629, 10 pages.
[32] M.S. Nejad, M. Khatami, G. Hosein, S. Bonjar, Streptomyces somaliensis mediated green synthesis of silver nanoparticles, Nanomed. J., 2 (2015) 233–238.
[33] G. Sundaraselvan, S.D. Quine, Green synthesis of zinc oxide nanoparticles using seed extract of *Murrayakoenigii* and their antimicrobial activity against some human pathogens, J. Nanosci. Tech., 4 (2017) 289–292.
[34] Y. Zang, R. Farnood, Photocatalytic activity of AgBr/TiO_2 in water under simulated sunlight irradiation, App. Cata. B: Environ., 79 (2008) 334–340.
[35] H.K. Farag, R.M.M. Aboelenin, N.A. Fathy, Photodegradation of methyl orange dye by ZnO loaded onto carbon xerogels composites, Asia-Pacific J. Chem. Eng., 12 (2017) 4–12.